Sulfur-Doped Cubic Mesostructured Titania Films for Use as a Solar Photocatalyst

Yuli Xiong,[†] Daping He,[‡] Robben Jaber,[†] Petra J. Cameron,[†] and Karen J. Edler[†,]*

[†] Department of Chemistry, University of Bath, Claverton Down, Bath BA2 7AY, UK.

[‡] School of Science, Wuhan University of Technology, Wuhan, Hubei 430070, P. R. China

ABSTRACT: Sulfur-doped titania thin films with cubic mesostructures were prepared by dip coating via the evaporation induced self-assembly route. The effect of sulfur doping on structure, morphology, porosity, optical properties and photocatalytic activity of the mesoporous films were studied. Compared to undoped titania films, the S-doped films showed better long range ordering, bigger pore size, higher porosity, less shrinkage of the structure during calcination, a red-shift of the band gap and a more hydrophilic surface. These characteristics led to an improved photocatalytic activity, when the S-doped and undoped titania films were tested for degradation of methylene blue in aqueous solutions under the irradiation of 1 sun from a solar simulator. The photocatalytic activity of the sulfur doped titania film was stable during three consecutive experiments under solar light irradiation, confirming the mechanical stability and reusability of the doped nanostructured thin film photocatalysts.

Introduction

It is well known that titania is an efficient photocatalyst under irradiation by UV light, however UV light only accounts for 3 % of the solar spectrum. Doping of titania has proven to be an effective way to extend the spectral response to visible light and is of considerable interest for many technological applications.[1-2] However, due to some drawbacks of metal-doped titania (such as potential metal leaching and photocorrosion), non-metal-doped materials are considered a more environmentally-friendly and effective approach. A number of experimental and theoretical studies have been focused on dopants such as N, B, F, C, P, or S, and codoping.[1-4] Since the synthesis of visible light-activated sulfur-doped titania was first reported by Umebayashi et al.,[5] sulfur doping has attracted extensive attention to enhance the photocatalytic activity of titania under visible-light irradiation.[6-10] S-doped titania nanoparticles have previously been fabricated using different sulfur sources and preparation methods, but the use of a titania powder as a photocatalyst requires its later separation from the solvent. Studies regarding S-doped titania thin films are much less developed. Dunnill et al. fabricated S-doped titania films by atmospheric pressure chemical vapor deposition using $TiCl_4$, ethyl acetate and carbon disulphide.[11] Pore et al. prepared S-doped titania films by atomic layer deposition using $TiCl_4$, H_2S and water.[12] Yamamoto et al. made S-doped titania films by pulsed laser deposition using a TiS_2 target.[13] All of these films were prepared via gas phase thin film deposition, which requires specific equipment. Sol-gel methods in contrast have been intensively employed to synthesize many metal oxide materials due to several advantages, such as low cost and low operating temperature, high chemical homogeneity and purity, and the possibility to control material morphology at the nanoscale. Disordered porous S-doped titania films have been reported by Han et al. made by a sol-gel method from dip coating with nonionic surfactant to control

nanostructure. In these films an inorganic sulfur source was used (H_2SO_4).[14-15] The earlier paper discussed the effects of calcination temperature[13] while a second paper investigated the influence of solvent on the physicochemical properties of the S-doped titania film.[14] However, the influence of S-doping on the physicochemical properties of ordered mesoporous titania films has not so far been discussed.

Porous films, especially with an organized mesostructure, can be efficient photocatalysts due to the highly organized pore structures allowing high surface areas and rapid diffusion through the material.[16] It is also expected that films with a cubic mesostructure would offer higher photocatalytic efficiency than those with a 2D hexagonal mesostructure, since the mesopore channels of cubic mesostructures are open on the surface of the film regardless of the mesophase orientation, whereas those of 2D hexagonal mesophases are parallel to the substrate and difficult to access.[17-19] One of the most promising methods to prepare ordered mesoporous films is the evaporation-induced self-assembly (EISA) route, which was pioneered by Brinker et al.[20] and adapted by Stucky and coworkers[21] and the Grosso group[22] for titania. High-quality mesoporous titania anatase thin films can be easily and reproducibly prepared via dip or spin coating methods, using inorganic precursors directed by surfactant templates and subsequent template removal.[23-25] However, few mesostructured titania films with a non-metal dopant have been reported,[26] and no S-doped titania with an ordered mesostructure has been reported, so far as we know.

In this work, S-doped titania films with a cubic mesostructure and ultrahigh surface area formed using dip coating are reported. S-doped mesoporous titania thin films were templated by Pluronic P123 using the EISA approach with sulfuric acid as the sulfur source in the initial sol. The effect of S-doping on the physicochemical properties of titania films were studied by small angle X-ray

scattering (SAXS), grazing incident SAXS (GISAXS), XRD, TEM, Field-Emission SEM, energy dispersive spectrometry (EDX), X-ray photoelectron spectroscopy (XPS), TGA, N_2 sorption isotherms, ellipsometry, UV–Vis adsorption and transmission, water contact angle measurements, and solar photocatalytic activity. Compared to an undoped film, the S-doped titania film has superior properties, such as a more ordered mesostructure, bigger pores, higher porosity, narrower band gap and better hydrophilicity, which contributed to more efficient visible-light photocatalytic activity.

Experimental

Synthesis of S-doped titania thin films

All chemicals were used as supplied. The films were prepared using a method that was modified from that of Alberius et al.[21] 1.0 g of Pluronic P123 (Sigma-Aldrich, MW ~5800) was dissolved into 12.0 g absolute ethanol (AR, Sigma-Aldrich) and a mixture of 2.86 g HCl (Fisher, 32%) and 0.2 ml H_2SO_4 (Fisher, 98%) was added. Then the solution was stirred vigorously for 3 hrs at room temperature. 5.36 g titanium tetraisopropoxide (TiPr, Acros, 98%) was added drop by drop under vigorous stirring. The precursor solution was stirred for another 30 min before it was used. To make a comparison, a precursor solution without adding H_2SO_4 was used to make an undoped titania film. There was essentially no difference in acidity between the two solutions as the overall acid concentration was ~1.7M for the sulfuric acid containing solution and ~1.6M for the undoped version.

Silicon wafers or microscope slides were cleaned and used as the substrates. A silicon wafer was normally used if not otherwise specified. Dip-coating was performed using a withdrawing speed of 60 mm/min, using a computer controlled Nima dip coater, model DSG-75. As soon as the

withdrawal of the substrate from solution was complete, each sample was placed into a fridge maintained at a temperature of 7 °C and 22 % relative humidity for 24 hrs, then moved into an oven at 40 °C and 55% relative humidity for 24 hrs and finally aged at 100 °C and 22 % relative humidity for 24 hrs. After that, films were heated at 350 °C for 2 hrs with a ramp speed of 1 °C/min to remove the template. The final calcination step was taken at 450 °C for 15 minutes with a ramp speed of 5 °C/min to crystallize the structure. Films were prepared on at least five separate occasions to complete the full set of characterization experiments, and gave comparable results for XRD and SAXS/GISAXS suggesting the synthesis is reproducible.

Characterization of S-doped titania thin films

The morphology of the film samples was observed by a Hitachi Field-Emission SEM (FESEM) S-4800 operated at 10 kV. The elemental analysis and mappings were recorded using energy dispersive spectroscopy (EDS) on the FESEM. Sulfur-doped thin film compositions were obtained by XPS using a Thermo ESCALAB 250 instrument equipped with a monochromatic Al Ka X-ray source ($h\nu$ = 1486.6 eV). The operating power was 150 W and the spot diameter 500 μm. An ellipsometer (alpha-SE Ellipsometer from J.A. Wollam Co.) was used to study the film thickness and the refractive index of the films. Results were fitted using a model for absorbing films on silicon contained in the CompleteEASE software. Absorbance of films on glass vs. air was recorded using a UV/Vis spectrometer (Varian, Cary 50 Probe). Films containing surfactant were scratched from substrates and analyzed by TGA using a Perkin Elmer TGA 7 thermogravimetric analyzer. GISAXS experiments on S-doped titania film samples before and after calcination were performed to observe the film structure on the I07 beamline at the Diamond Light Source. GISAXS patterns were collected at an incident angle of 0.25°, using an energy of 12.5 keV (= 1.0 Å). Calcined films, scratched from the substrate to make powders

were tested using SAXS (Anton Paar SAXSess, Cu Kα radiation), XRD (Brucker D8 powder diffractometer with Cu Kα radiation) and TEM (JEM-2100F) to check the crystal structure and long range ordering. N_2 ad/desorption isotherms were taken to check the surface area and pore size distribution using a BELSORP-mini II after the powdered calcined film samples were degassed at 150 ºC for 4 hrs. A water droplet on the films was recorded using a Veho Discovery Microscope (VMS-004 Deluxe) to obtain the water contact angle.

The photocatalytic activity of the thin films was monitored by immersing the samples into 100 ml of 5 μM methylene blue aqueous solution under 1 sun illumination from a TS Space Systems solar simulator. The films were allowed to reach an adsorption-desorption equilibrium for 1 hr before irradiation. The concentration of methylene blue solution was determined by measuring the visible light absorbance at 650 nm using an UV/Vis spectrophotometer. 3 mL of solution was used for testing and returned to the solution after measurement.

Results and Discussion

According to the report of Alberius et al.,[21] titania films with a cubic mesostructure can be obtained when the template volume fraction of Pluronic P123 is in the range of 29-36%. In our case, the template volume fraction is 31 %, thus a cubic structure is expected.

Figure 1 shows the SAXS patterns of the S-doped and undoped titania before (A) and after (B) calcination. Both of the as-prepared samples had a shoulder at ~0.039 $Å^{-1}$. From the SAXS patterns of the calcined samples, it is obvious that S-TiO_2 has a much more ordered structure than TiO_2. The titania only has a single broad peak at ~0.042 $Å^{-1}$ indicating a disordered structure, but the S-TiO_2 has two strong peaks at 0.036 and 0.042 $Å^{-1}$ and one broader peak at ~0.07 $Å^{-1}$, suggesting a cubic structure ($Pn\bar{3}m$ symmetry) with a d-spacing of 16.5 nm. From the

position of the peak or shoulder in the undoped titania sample, a shift to lower q (from 0.039 to 0.042 $Å^{-1}$) was observed, suggesting shrinkage of the titania network after the removal of template. However little shift was observed for S-doped titania, as it had a broad unresolved peak around 0.039 $Å^{-1}$ before calcination and two strong peaks at 0.037 and 0.041 $Å^{-1}$ after calcination. For the as-prepared samples, in both cases only one broad peak was displayed. This is probably because the mesostructure of titania/template is not fully condensed prior to calcination and could be partially disordered by the process of scratching the film away from the substrates.

Figure 1 also displays the GISAXS and corresponding intensity profiles in the Q_Z and Q_{XY} directions, of patterns taken from the S-TiO_2 film before (C) and after (D) calcination. Before calcination (Figure 1C), the pattern from the film shows two spots in the vertical direction and two arcs in the scattering. In the cut taken in the vertical direction, as well as peaks at 0.036 and 0.046 $Å^{-1}$, there is one more peak at ~0.067 $Å^{-1}$ and a shoulder at ~ 0.118 $Å^{-1}$, which is in accordance with the SAXS pattern of the film after calcination. These suggest that the film has a cubic mesostructure ($Pn\bar{3}m$ symmetry) and the peaks are indexed as the (110), (111) and (200) planes, according to the ratio of peak positions. The unit cell size remains almost the same before and after calcination. There is only one peak at 0.036 $Å^{-1}$ and a shoulder at ~ 0.070 $Å^{-1}$ visible in the in-plane direction cut, this is because the in-plane cut was taken at Q_Z=0.04 $Å^{-1}$ due to the position of the beam-stop and more diffraction peaks would normally be seen at lower Q_Z values. After calcination (Figure 1D), the film still showed a well-defined structure. In the cut taken in the vertical direction, the degree of ordering became worse, as the clear ring that appeared in the as-prepared sample became broadened and shifted to a larger Q value ~0.088 $Å^{-1}$ after calcination. The peak at 0.046 $Å^{-1}$ corresponds to the (111) plane, which is the same as in the as-prepared sample. In this symmetry there should also be another peak at 0.036 $Å^{-1}$, but this peak is

blocked by the beam-stop. In the cut taken in the in-plane direction, there is one peak at 0.036 $Å^{-1}$ and a broad shoulder at ~0.062 $Å^{-1}$, which is quite similar to the as-prepared sample. The peaks appear stronger and more well-defined than in the as-prepared pattern due to the increased contrast between pore and wall domains after the removal of template. According to the ratio of d-spacings, the peak at ~0.062 $Å^{-1}$ is indexed as the (211) plane of the $Pn\bar{3}m$ micellar cubic phase. Noticeably, no shrinkage of the mesostructure after calcination was observed for the S-doped titania film. The doping with sulfur helps to maintain the mesostructure, despite it being very common for pure templated titania films to show a shrinkage in the vertical direction after calcination.[27] The GISAXS results for the calcined S-doped film are in agreement with the SAXS results. The size of the cubic unit cell for the as-prepared and calcined S-doped titania film is a=b=c=24.7 nm in both cases.

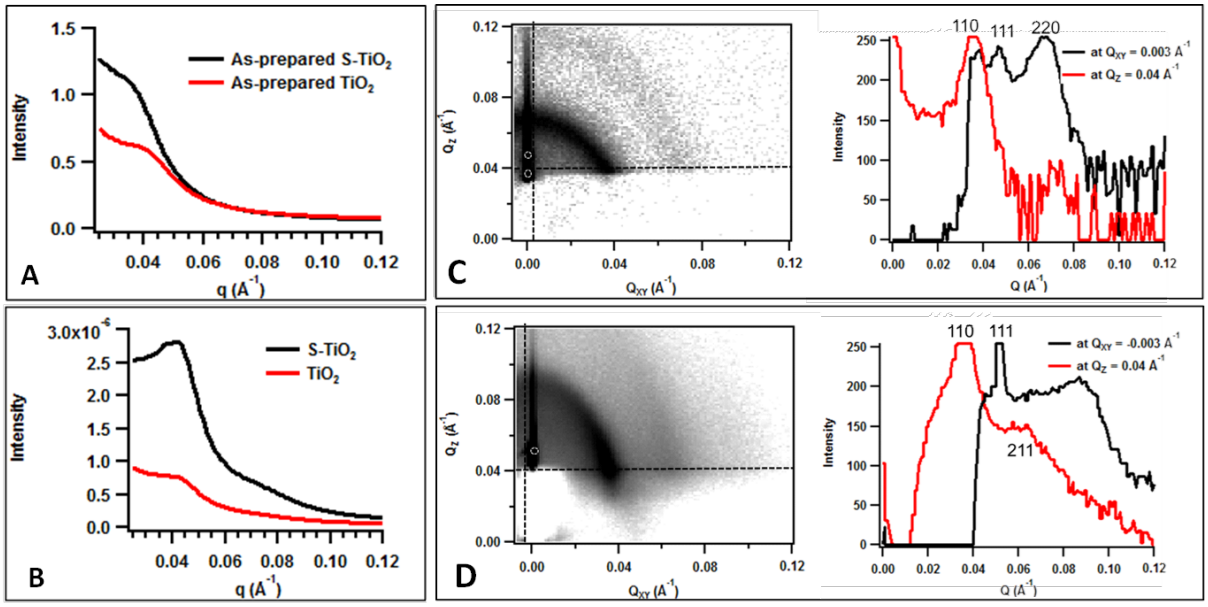

Figure 1 SAXS curves of S-TiO2 and TiO2 before (A) and after calcination (B); GISAXS image (left) and corresponding intensity profile in the Q_Z and Q_{XY} directions as indicated by the lines on the GISAXS patterns (right) of S-TiO_2 film before (C) and after calcination (D)

The XRD curves for the S-TiO_2 and TiO_2 film after removal from their substrates as a powder are shown in ESI Figure S1†. The primary peak of the anatase phase at $2\theta = 25°$ was obviously found in both samples. The TiO_2 film is better crystallized than the S-TiO_2 film, since only one peak was clearly observed in the S-TiO_2 XRD pattern, with a relatively broad peak width, indicating that the mesostructured wall is composed of nanosized anatase crystallites. Also no other peaks from other phases were observed, suggesting the sulfur was doped into the lattice rather forming segregated phases. The crystal size, calculated according to the Scherrer equation,[28] was around 4.5 nm for S-TiO_2 and 6.0 nm for TiO_2. These suggest that the incorporation of sulfur inhibits the crystal growth of the embedded anatase TiO_2 in the walls of the mesostructure during calcination, resulting in a smaller crystallite size for the doped materials. The smaller crystallite size in turn means that the S-doped crystals can be effectively accommodated within the walls of the mesostructure, leading to the improved mesostructural porosity observed in the doped materials.

The porous structure and the morphology of the materials were further studied by TEM (Figure 2). Figures 2A and B shows a well-ordered pore structure in the S-doped titania from the (111) and (110) orientation of the cubic phase ($Pn\bar{3}m$ symmetry) with a linear array of pores arranged at regular intervals. The orientation and pore entrance of the individual pores are clearly visible. The high level of ordering of the cubic $Pn\bar{3}m$ phase was also demonstrated by the Fourier Transfer images of the mesostructure of the film. The d-spacing of the (110) direction in the cubic mesostructured film was found to be ~16 nm, which is in accordance with SAXS and GISAXS results. In Figure 2C, the pores have a well-defined shape. The mesostructured film has 7 - 9 nm pores and 4 - 6 nm walls. Also, we do not observe any unidirectional shrinkage of the cross-sectional pore structure, which helps retain the well-ordered structure even after

calcination. From Figure 2D, a typical pore and walls is displayed at high magnification. The pore has a very regular shape and is composed of a 7.0 nm diameter void and 4.7 nm thick walls. It can be noticed that the wall areas are composed of highly-crystalline anatase nanoparticles, as the titania lattice spacing of 0.35 nm corresponding to the (101) anatase crystal plane is clearly seen in the nanoparticles, which is in good agreement with the XRD studies. The anatase nanoparticles are randomly embedded into the mesoporous walls of the thin films. In comparison, the pure titania material had a wormlike mesostructure from Figure 2E. In Figure 2F, the pore unit cell does not show pores with a well-defined shape and the pore size is smaller due to the larger crystallites in the mesopore wall domains. Usually, the anisotropic crystallization and growth of crystalline particles are apt to produce particles which exceed the geometry of the inorganic framework and will lead to the obvious distortion or deterioration of the ordered mesopore structures.[29] In our case, the anatase crystals in S-doped titania film have a relatively smaller size than in the pure titania film and so occupy the limited space within the channel walls, resulting in a crystallized but also well-ordered mesostructure.

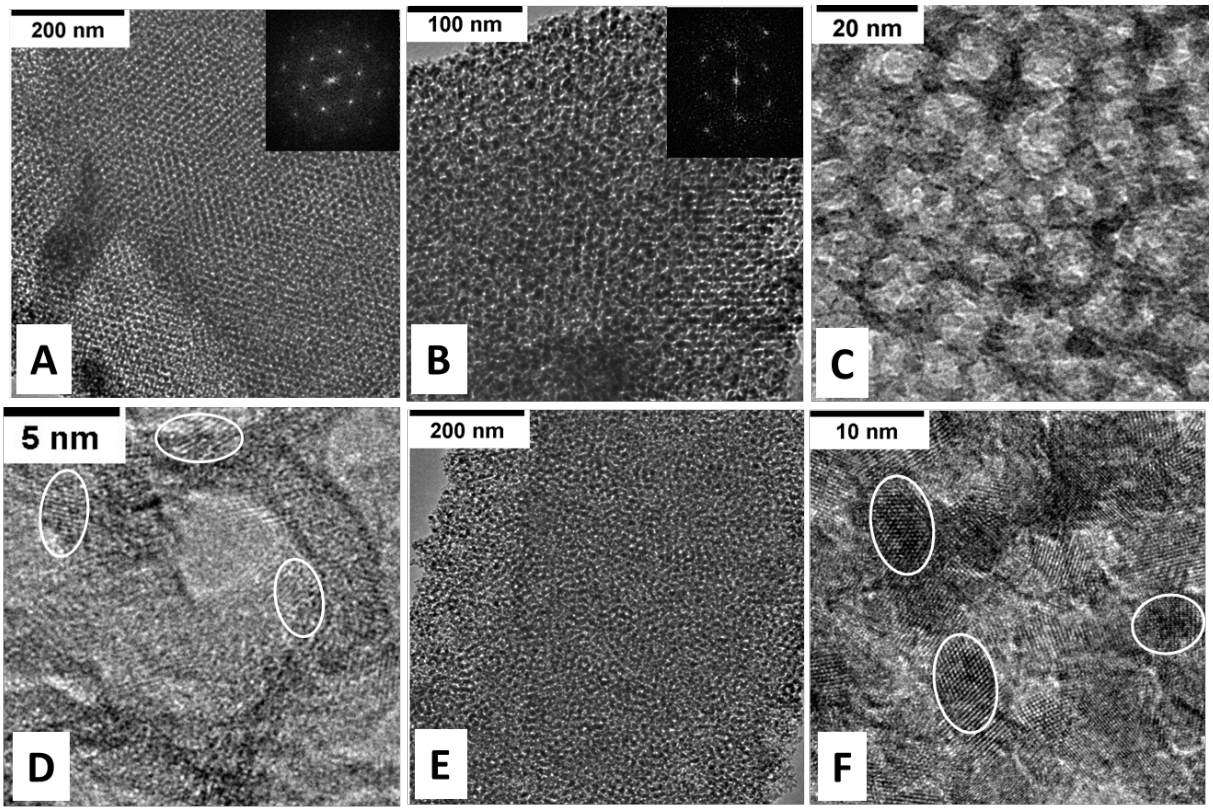

Figure 2 TEM images of S-doped (A, B, C, D) and undoped titania (E, F)

Figure 3 shows the FESEM images of S-doped (A) and undoped (B) titania films. Both of them display a smooth surface and have a high porosity with the mesopores open to the film surface, which may help the access of species to reactive sites within the pores. Compared to the titania film, it is clearly seen that the S-TiO_2 film has an extremely flat surface and the pore openings are arranged perpendicular to the surface plane, are uniform in size and regularly distributed. From the magnified images, many pores in the pure titania film collapsed due to the crystallization of the pore walls during calcination.[24] Noticeably, the S-TiO_2 film retains a good pore structure with the pore diameter around 7.5 - 9.5 nm, wall thickness around 5.5 - 7.5 nm and the pore repeat spacing around 16-18 nm. These correspond with the SAXS, XRD and TEM results. EDX elemental analysis (Figure 3C) identified the presence of sulfur in the doped titania film, giving an atomic ratio between Ti and S of 1:0.15. The relatively low signal intensity of O,

Ti and S atoms is because the signal of the Si substrate is too strong. Elemental mappings of O, Ti and S show that these elements are uniformly distributed over the whole region, demonstrating the good dispersion of the sulfur in the titania film.

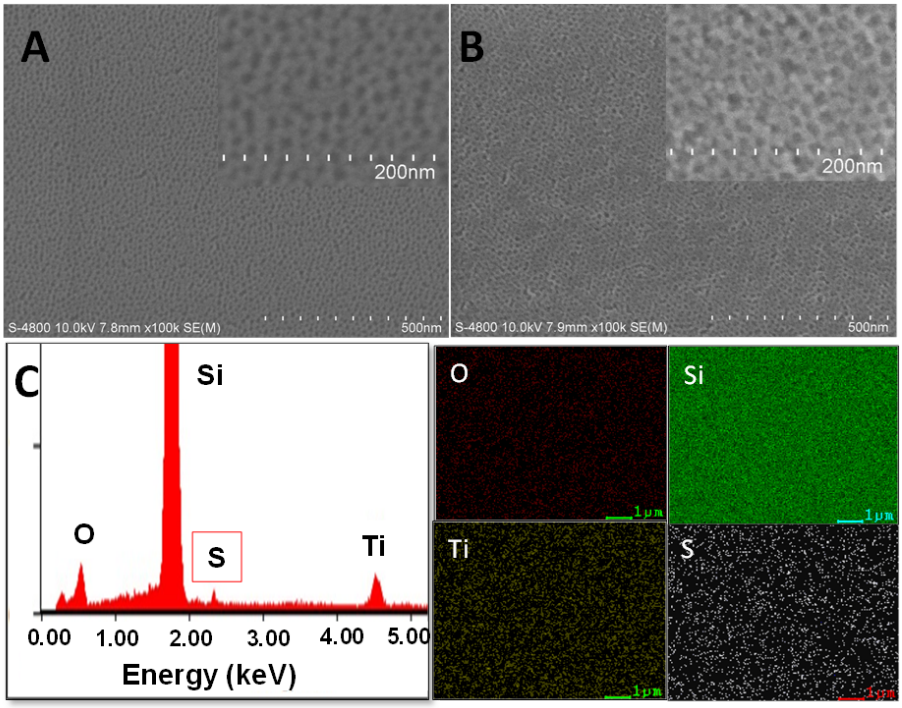

Figure 3 FESEM images of S-doped (A) and undoped (B) titania films; EDS and element mapping of S-doped titania film (C)

XPS was exploited in order to identify the presence of sulfur species in the titania films, as shown in Figure 4. Figure 4A shows a wide-scan survey spectrum of the S-doped film where the dominant O, Ti, and S elements can be identified through their corresponding O 1s, Ti 2p, and S 2p peaks. The C 1s is probably from the contamination of sample after exposure in air or a small amount of residual carbon from the template. By comparison with other studies,[15, 30-31] the two peaks at 168.2 and 169.9 eV in Figure 4B can be assigned to S^{4+} and S^{6+} states, contributing to the substitution of Ti^{4+} by S ions. No peaks were found around 160-163 eV, which corresponds

to the Ti-S bond where S atoms replaced O atoms. This is because the ionic form of the sulfur dopant is dependent on the starting material. When TiS_2 is used as the starting material, most of the sulfur in TiS_2 was oxidized and the residual sulfur would naturally remain as S^{2-}.[5] In our work, however, we used TiPr and sulfuric acid as the titanium and sulfur source respectively. Anionic sulfur doping may be difficult to carry out because of the larger energy required for the formation of Ti-S bond than Ti-O bond, as the S^{2-} (1.7 Å) has a significantly larger ionic radius compared to that of O^{2-} (1.22 Å). Thus, substitution of Ti^{4+} by S ions is chemically more favorable than replacing O^{2-} with S^{2-}, which is confirmed by our XPS results. The atomic ratio between Ti and S is 1:0.13, which is similar to the EDS results from these materials.

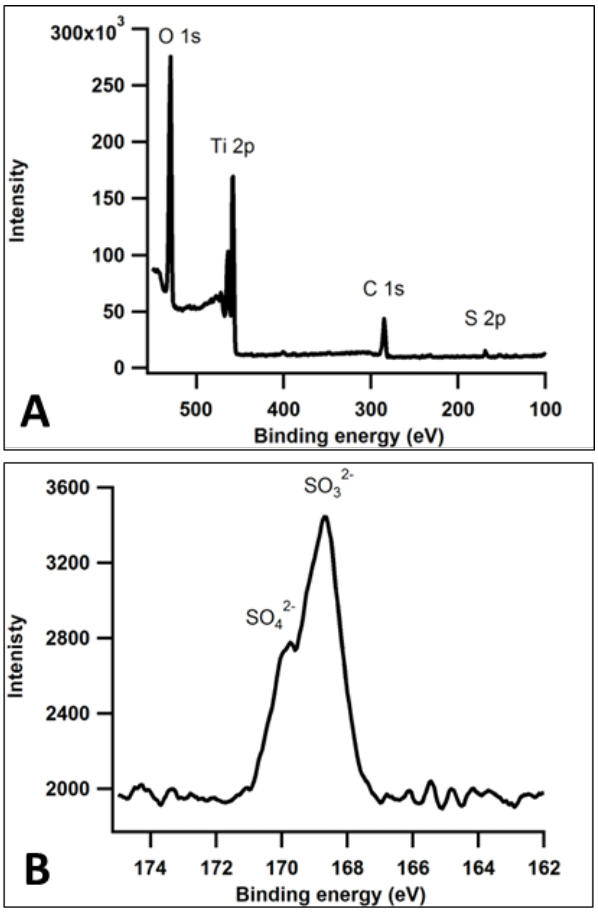

Figure 4 XPS survey spectra (A) and S 2p high-resolution spectra (B) of S-doped film.

Figure 5 shows the nitrogen sorption isotherms and pore size distribution of S-doped and undoped titania films. Their isotherms can be classified as type IV, which is characteristic of mesoporous materials. Also, they show a sharp capillary condensation step at a relative pressure of 0.55-0.75, suggesting a narrow pore size distribution.[32] A pronounced H1-type desorption hysteresis loop suggests the existence of large mesopores with open-ended ended cylindrical shapes in these samples.[32] The shapes of the isotherms for both samples look similar, although the hysteresis loop is a little smaller and shifts to lower relative pressure for pure titania compared to the S-doped sample, which suggests a smaller pore size and broader pore distribution. BJH pore-size analyses performed on the adsorption branch show that the S-doped and undoped titania exhibit a mean pore size of 7.0 nm and 6.2nm, respectively. Excluding macropores, the pore size distribution of S-doped titania is more uniform and narrower than that of the undoped titania film. The titania films show a small number of pores in the range of 20-70 nm probably from the fusing of small pores during the calcination,[33] or from gaps between crystallites. Although bigger pores always result in a smaller surface area, they share similar high BET surface areas, at 190 m^2/g for the S-TiO_2 and 187 m^2/g for the undoped TiO_2 film (commercial P25 titania nanoparticles have a surface area around 50 m^2/g). The pore volumes are 0.50 cm^3/g for S-TiO_2 and 0.55 cm^3/g for TiO_2. The lower pore volume of S-TiO_2 is due to the lack of macropores in this material. These results are summarized in Table 1.

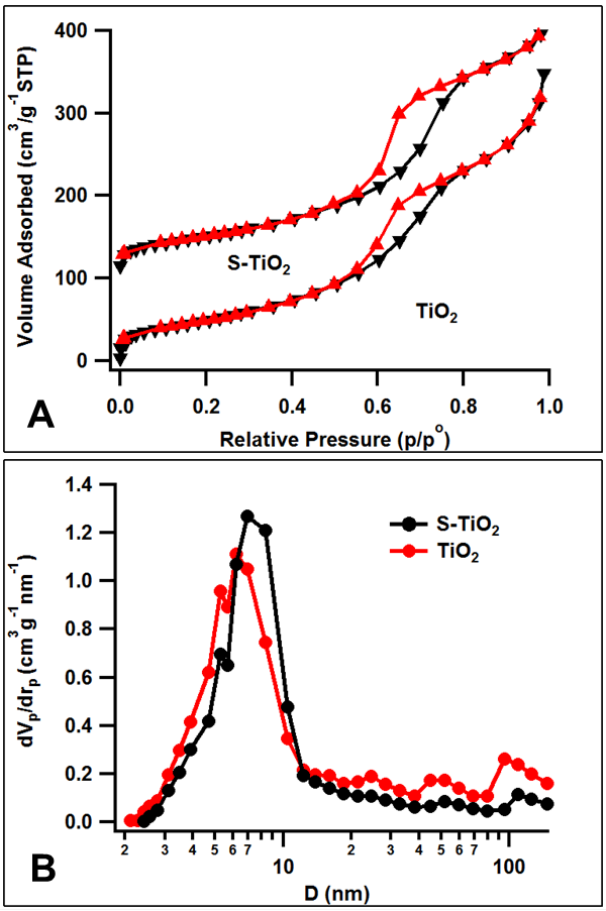

Figure 5 N_2 sorption isotherms (A) and pore size distribution (B) of S-TiO_2 and TiO_2 after calcination.

TGA curves of doped and undoped titania are displayed in ESI Figure S2†. In the temperature range of 40-180 °C, weight loss occurs due to the evaporation of solvent. The mass loss of S-doped titania (~13%) is higher than pure titania (~5%), because more water was left in the as-prepared sample. The sulfuric acid in solution would become concentrated during the evaporation steps and ageing process, and concentrated sulfuric acid is known to assist the retention of water in the film. Then, a sharp decrease occurs in the range of 180 - 300 °C from the combustion of the template. After this, a small amount of weight loss happens due to the continuous removal of residual organic and the transformation of amorphous phase into anatase

phase at higher temperatures.[34-35] It is clear that most of the organic template is removed from the films upon calcination at 300 °C, which is in good agreement with results reported in the literature.[9, 24] After calcination at 350 °C, the remaining mass of the inorganic network for the S-doped titania film is 62 % and 68 % for TiO_2. Considering the weight differences of water found in the as-prepared samples, the amount of inorganic species in the as-prepared films is similar.

Table 1 also lists the results from modeling of ellipsometry measurements. Both of the films before calcination show a similar thickness around 415 nm. After calcination, the film thickness decreased due to the combustion of template and shrinkage of the inorganic network. The titania film has a thickness of 215 nm, which corresponds reasonably well with work by others, as the films were aged under a medium relative humidity during synthesis.[23] The S-doped film has a greater thickness of 317 nm, which is increased by almost 50 % compared to that of the undoped film. The shrinkage of the film was around 48 % for the undoped film and only 25 % for S-doped titania according to the film thickness, indicating the S-modification favors the retention of the mesoscopic structure of the films. The refractive index found from model fitting was used to calculate the porosity of the mesoporous TiO_2 thin films through the following equation:[36]

$$P = \left(1 - \frac{n^2-1}{n_T^2-1}\right) \times 100\% \qquad (1)$$

where n is the refractive index measured by ellipsometry and n_T is the refractive index of anatase (n_T = 2.55). For the S-doped titania film, the refractive index is 1.47 while that for the pure titania film is 1.55. The porosity for the titania film is 74% and for the S-doped film is 78%. To the best of our knowledge, this is the highest porosity of mesoporous titania films so far reported.[27, 37-38]

Table 1 Textural properties of S-doped and undoped titania films

Sample	Thickness before calcination (nm)	Thickness after calcination (nm)	Porosity (%)	Pore size (nm)	S_{BET} (m^2/g)	Pore volume (cm^3/g)	Crystallite Size (nm)
S-TiO_2	418±2	317±1	78±1	7.0±0.2	190±2	0.50±0.01	4.5±0.2
TiO_2	412±2	215±1	74±1	6.2±0.2	187±2	0.55±0.01	6.0±0.2

Figure 6 shows the absorbance and transmission of S-doped and pure titania films coated on glass slides. The S-modification improved the light absorbance over the whole spectral range. From the absorbance curves, a clear shift of the band onset in the direction of the visible region of the spectrum is observed for the S-doped samples, suggesting the dopant results in band-gap narrowing effects.[5, 39-40] The transmission also confirmed the red-shift of the absorbance of the film arising from the doping modification. S-TiO_2 has a higher absorbance and 10 % lower transmission compared to the undoped film over the whole visible region, probably due to the doping effects and the ~47 % increase in thickness indicated by the ellipsometry measurements above.

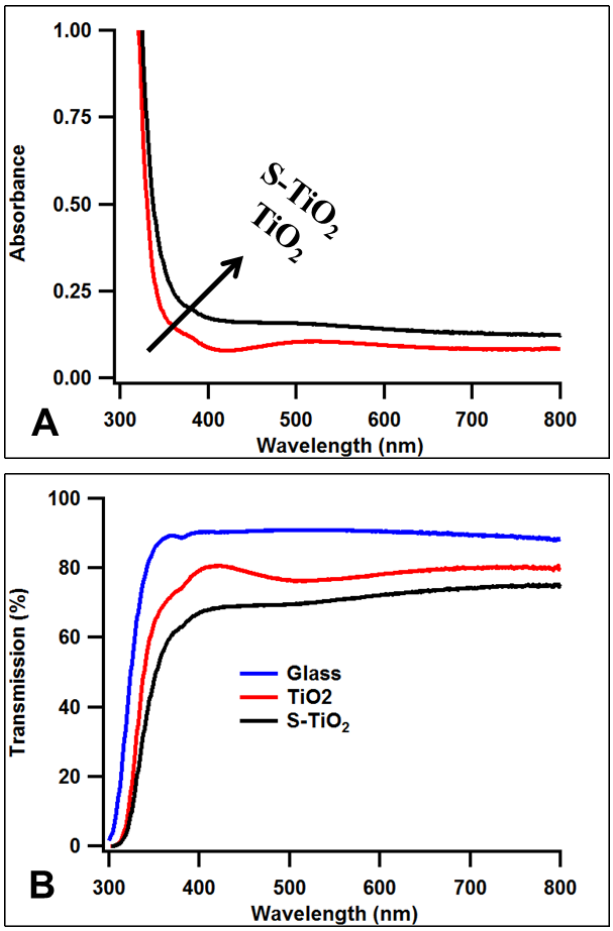

Figure 6 Absorbance (A) and transmission (B) of S-doped and undoped titania films on glass slide

The surface hydrophilicity of S-doped and undoped films were measured via comparison of water contact angles, as shown in ESI Figure S3†. The contact angle of S-doped and undoped films were 23° and 47°, respectively, which will affect the photocatalytic activity. Photocatalytic activity is closely related to hydrophilicity, because water OH groups adsorbed on hydrophilic surfaces form the active species •OH, which enhances the photocatalytic activity.[41] Here, the water contact angle on the S-doped film is decreased by 24° compared to that of the undoped titania film; this is a relatively large decrease since no further treatment was carried out on the

film surface. To achieve a more hydrophilic surface, Sakai et al. used an anodic polarization treatment to obtain a 7 - 15° decrease in the water contact angle,[42] while Yu et al. adopted a HCl solution treatment to cause an ~7° decrease of the water contact angle on a titania surface.[43]

The photocatalytic activity of these films under 1 sun irradiation from a solar simulator was investigated. In Figure 7, the S-TiO_2 film exhibited higher activity for the degradation of methylene blue than the TiO_2 film, demonstrating the positive effect of the S-modification. Although the S-TiO_2 anatase structure is less well crystallized than the undoped sample, which is expected to slow the transfer of photocharges from bulk to surface,[44] the improvement in photocatalytic efficiency can be explained by several factors. S-TiO_2 has a more well-defined mesoporous structure and the ordered mesopore channels facilitate fast intraparticle molecular transfer. Bian et al. fabricated Bi doped TiO_2 nanocrystalline films with an ordered mesoporous structure by the EISA method to use as a visible light photocatalyst,[45] while Li et al. similarly fabricated Ce-doped TiO_2 nanoparticles via the EISA route, also for photocatalysis.[46] Both papers report that the ordered mesoporous channels facilitated diffusion of the reactant molecules.[45-46] The S-modification also resulted in an increase in the pore size and porosity, and this larger pore size will facilitate the access and diffusion of large organic molecules within the pores.[47-48] Additionally, sulfur doping resulted in a slight red-shift of the band gap of the film, thus, the catalyst could more be easily activated by visible light than the undoped material. Finally, sulfur doping induced formation of a more hydrophilic film surface, which allows aqueous solutions to wet the pore surfaces more efficiently. This allows more reactive •OH groups to be generated, thus an increase in hydrophilicity benefits the photocatalytic activity, even for degradation of hydrophobic molecules.[40] To test the mechanical stability and reusability of the doped nanostructured thin film photocatalysts, the S-TiO_2 films were used repeatedly for

photocatalysis. After use in three cycles for the photocatalytic degradation of methylene blue, the S-doped titania films show a small loss of photocatalytic activity, as shown in the inset of Figure 7. Other authors have ascribed similar loss of activity to the adsorption of non-degraded compounds on the photocatalyst surface or to changes in the surface structure of the photocatalyst caused by interactions with reaction intermediates.[49-50] The retention of photocatalytic activity indicates that these films are mechanically stable and reusable under these experimental conditions, which is important to any eventual practical environmental applications.

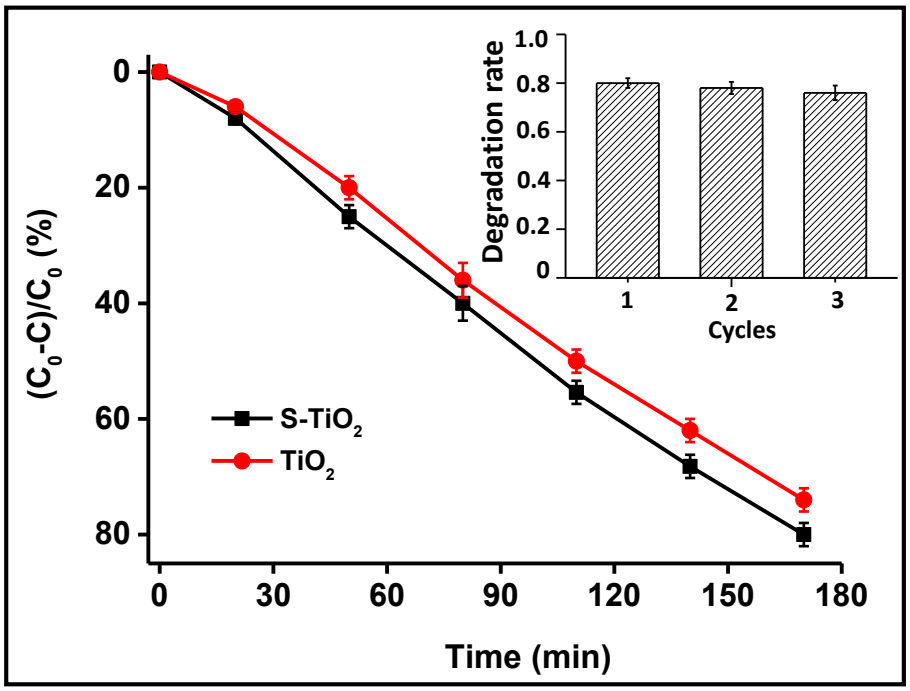

Figure 7 Photocatalytic degradation of methylene blue (MB) aqueous solution on S-doped and undoped films (error bars based on measurement of three samples at each reaction time); Three cycles for the photocatalytic degradation of methylene blue using the same S-doped titania film (inset).

Conclusions

S-doped titania thin films with a cubic $Pn\bar{3}m$ phase mesostructure were prepared and applied in sun-light-driven photocatalysis. Using sulfuric acid as the sulfur source, led to successful and uniform doping of sulfur into the titania films. Sulfur doping modified the film properties compared to undoped TiO_2 films prepared using the same method. The S-TiO_2 film had a thickness of 317 nm and contained an anatase phase in the walls, had large, open pores (7.0 nm diameter), a high surface area (190 m^2/g), high porosity (78%) and relatively little thickness shrinkage after calcination (25%). However, the pure titania film had a wormlike mesostructure and exhibited a large amount of pore collapse due to the growth of larger crystallites in the wall domains compared to those in the S-doped film. Pure titania films had smaller pores and underwent greater shrinkage in thickness after calcination. The photocatalytic activity was measured via degradation of methylene blue aqueous solution under a solar simulator and the S-doped titania film had an improved efficiency compared to that of the undoped film despite having a similar surface area. This improved photocatalytic efficiency arises because the S-modification favors formation of films with a better ordered mesostructure, bigger pore size, higher porosity, a red-shift of the band gap and a more hydrophilic surface. These suggest that S-doping and optimization of the mesostructure of titania films is a promising way to enhance the photocatalytic activity of these materials under sunlight.

ASSOCIATED CONTENT

The supporting information is available free of charge via the Internet at http://pubs.acs.org.

XRD, TGA data for S-doped and undoped titania films, and images showing the contact angle of water resting on S-doped and undoped titania films. (PDF)

AUTHOR INFORMATION

Corresponding Author

* Fax: 44 1225 386231; Tel: 44 1225 384192; E-mail: K.edler@bath.ac.uk

Author Contributions

The manuscript was written through contributions of all authors. All authors have given approval to the final version of the manuscript.

Notes

The authors declare no competing financial interest.

ACKNOWLEDGMENT

This work was supported by an Overseas Student Scholarship from University of Bath and by the Chinese Scholarship Council. We also thank Diamond Light Source for the allocation of beamtime on beamline I07 (experiment number SI7608) and Dr Tom Arnold and Dr Jonathan Rawle for assistance with running this experiment.

REFERENCES

1. Banerjee, S.; Pillai, S. C.; Falaras, P.; O'Shea, K. E.; Byrne, J. A.; Dionysiou, D. D., New Insights into the Mechanism of Visible Light Photocatalysis. *J. Phys. Chem. Lett.* **2014,** *5*, 2543-2554.

2. Pelaez, M.; Nolan, N. T.; Pillai, S. C.; Seery, M. K.; Falaras, P.; Kontos, A. G.; Dunlop, P. S. M.; Hamilton, J. W. J.; Byrne, J. A.; O'Shea, K.; Entezari, M. H.; Dionysiou, D. D., A Review on the Visible Light Active Titanium Dioxide Photocatalysts for Environmental Applications. *Appl. Catal. B* **2012,** *125*, 331-349.

3. Portela, R., Non-metal Doping for Band-Gap Engineering. In *Design of Advanced Photocatalytic Materials for Energy and Environmental Applications*, Coronado, M. J.; Fresno, F.; Hernández-Alonso, D. M.; Portela, R., Eds. Springer London: London, 2013; pp 287-309.

4. Devi, L. G.; Kavitha, R., A Review on Non Metal Ion Doped Titania for the Photocatalytic Degradation of Organic Pollutants under UV/solar Light: Role of Photogenerated Charge Carrier Dynamics in Enhancing the Activity. *Appl. Catal. B* **2013,** *140-141*, 559-587.

5. Umebayashi, T.; Yamaki, T.; Itoh, H.; Asai, K., Band gap narrowing of titanium dioxide by sulfur doping. *Appl. Phys. Lett.* **2002,** *81*, 454-456.

6. Yu, J. C.; Ho, W.; Yu, J.; Yip, H.; Wong, P. K.; Zhao, J., Efficient Visible-Light-Induced Photocatalytic Disinfection on Sulfur-Doped Nanocrystalline Titania. *Environ. Sci. Technol.* **2005,** *39*, 1175-1179.

7. Schleife, A.; Rinke, P.; Bechstedt, F.; Van de Walle, C. G., Enhanced Optical Absorption Due to Symmetry Breaking in $TiO_{2(1-x)}S_{2x}$ Alloys. *J. Phys. Chem. C* **2013,** *117*, 4189-4193.

8. Abu Bakar, S.; Ribeiro, C., An Insight Toward the Photocatalytic Activity of S Doped 1-D TiO_2 Nanorods Prepared via Novel Route: As Promising Platform for Environmental Leap. *J. Mol. Catal. A* **2016,** *412*, 78-92.

9. Periyat, P.; Pillai, S. C.; McCormack, D. E.; Colreavy, J.; Hinder, S. J., Improved High-Temperature Stability and Sun-light-driven Photocatalytic Activity of Sulfur-doped Anatase TiO_2. *J. Phys. Chem. C* **2008,** *112*, 7644-7652.

10. Liu, R.; Ren, F.; Yang, J.; Su, W.; Sun, Z.; Zhang, L.; Wang, C., One-step Synthesis of Hierarchically Porous Hybrid TiO_2 Hollow Spheres with High Photocatalytic Activity. *Frontiers Mater. Sci.* **2016,** *10*, 15-22.

11. Dunnill, C. W.; Aiken, Z. A.; Kafizas, A.; Pratten, J.; Wilson, M.; Morgan, D. J.; Parkin, I. P., White Light Induced Photocatalytic Activity of Sulfur-doped TiO_2 Thin Films and Their Potential for Antibacterial Application. *J. Mater. Chem.* **2009,** *19*, 8747-8754.

12. Pore, V.; Ritala, M.; Leskela, M.; Areva, S.; Jarn, M.; Jarnstrom, J., H_2S ModifiedAtomic Layer Deposition Process for Photocatalytic TiO_2 Thin Films. *J. Mater. Chem.* **2007,** *17*, 1361-1371.

13. Yamamoto, S.; Takeyama, A.; Yoshikawa, M., Characterization of Sulfur-doped TiO_2 Films by RBS/C. *Nuclear Instruments Methods Phys. Res. B* **2006,** *242*, 377-379.

14. Han, C.; Pelaez, M.; Likodimos, V.; Kontos, A. G.; Falaras, P.; O'Shea, K.; Dionysiou, D. D., Innovative Visible Light-activated Sulfur Doped TiO_2 Films for Water Treatment. *Appl. Catal. B* **2011,** *107*, 77-87.

15. Han, C.; Andersen, J.; Likodimos, V.; Falaras, P.; Linkugel, J.; Dionysiou, D. D., The Effect of Solvent in the Sol–gel Synthesis of Visible Light-activated, Sulfur-doped TiO_2 Nanostructured Porous Films for Water Treatment. *Catal. Today* **2014,** *224*, 132-139.

16. Ismail, A. A.; Bahnemann, D. W., Mesoporous Titania Photocatalysts: Preparation, Characterization and Reaction Mechanisms. *J. Mater. Chem.* **2011,** *21*, 11686-11707.

17. Carreon, M. A.; Choi, S. Y.; Mamak, M.; Chopra, N.; Ozin, G. A., Pore Architecture Affects Photocatalytic Activity of Periodic Mesoporous Nanocrystalline Anatase Thin Films. *J. Mater. Chem.* **2007,** *17*, 82-89.

18. Pan, J. H.; Lee, W. I., Preparation of Highly Ordered Cubic Mesoporous WO_3/TiO_2 Films and Their Photocatalytic Properties. *Chem. Mater.* **2006,** *18*, 847-853.

19. Sakatani, Y.; Grosso, D.; Nicole, L.; Boissiere, C.; Soler-Illia, G. J. de A. A.; Sanchez, C., Optimised Photocatalytic Activity of Grid-like Mesoporous TiO_2 Films: Effect of Crystallinity, Pore Size Distribution, and Pore Accessibility. *J. Mater. Chem.* **2006,** *16*, 77-82.

20. Brinker, C. J.; Lu, Y.; Sellinger, A.; Fan, H., Evaporation-induced Self-assembly: Nanostructures Made Easy. *Adv. Mater.* **1999,** *11*, 579-585.

21. Alberius, P. C. A.; Frindell, K. L.; Hayward, R. C.; Kramer, E. J.; Stucky, G. D.; Chmelka, B. F., General Predictive Syntheses of Cubic, Hexagonal, and Lamellar Silica and Titania Mesostructured Thin Films. *Chem. Mater.* **2002,** *14*, 3284-3294.

22. Grosso, D.; Soler-Illia, G. J. de A. A.; Babonneau, F.; Sanchez, C.; Albouy, P. A.; Brunet-Bruneau, A.; Balkenende, A. R., Highly Organized Mesoporous Titania Thin Films Showing Mono-oriented 2D HexagonalChannels. *Adv. Mater.* **2001,** *13*, 1085-1090.

23. Crepaldi, E. L.; Soler-Illia, G. J. de A. A.; Grosso, D.; Cagnol, F.; Ribot, F.; Sanchez, C., Controlled Formation of Highly Organized Mesoporous Titania Thin Films: from Mesostructured Hybrids to Mesoporous Nanoanatase TiO_2. *J. Am. Chem. Soc.* **2003,** *125*, 9770-9786.

24. Choi, S. Y.; Mamak, M.; Coombs, N.; Chopra, N.; Ozin, G. A., Thermally Stable Two-Dimensional Hexagonal Mesoporous Nanocrystalline Anatase, Meso-nc-TiO_2: Bulk and Crack-free Thin Film Morphologies. *Adv. Func. Mater.* **2004,** *14*, 335-344.

25. Soler-Illia, G. J. de A. A.; Angelome, P. C.; Fuertes, M. C.; Grosso, D.; Boissiere, C., Critical Aspects in the Production of Periodically Ordered Mesoporous Titania Thin Films. *Nanoscale* **2012,** *4*, 2549-2566.

26. Soni, S. S.; Henderson, M. J.; Bardeau, J.-F.; Gibaud, A., Visible-light Photocatalysis in Titania-based Mesoporous Thin Films. *Adv. Mater.* **2008,** *20*, 1493-1498.

27. Grosso, D.; Soler-Illia, G. J. de A. A.; Crepaldi, E.; Cagnol, F.; Sinturel, C.; Bourgeois, A.; Brunet-Bruneau, A.; Amenitsch, H.; Albouy, P.; Sanchez, C., Highly Porous TiO_2 Anatase Optical Thin Films with Cubic Mesostructure Stabilized at 700 °C. *Chem. Mater* **2003,** *15*, 4562-4570.

28. Patterson, A., The Scherrer Formula for X-ray Particle Size Determination. *Phys. Rev.* **1939,** *56*, 978-982.

29. Wang, K.; Morris, M.; Holmes, J., Preparation of Mesoporous Titania Thin Films with Remarkably High Thermal Stability. *Chem. Mater* **2005,** *17*, 1269-1271.

30. Lee, H. U.; Lee, S. C.; Choi, S. H.; Son, B.; Lee, S. J.; Kim, H. J.; Lee, J., Highly Visible-Light Active Nanoporous TiO_2 Photocatalysts for Efficient Solar Photocatalytic Applications. *Appl. Catal. B* **2013,** *129*, 106-113.

31. Jalalah, M.; Faisal, M.; Bouzid, H.; Ismail, A. A.; Al-Sayari, S. A., Dielectric and Photocatalytic Properties of Sulfur Coped TiO_2 Nanoparticles Prepared by Ball Milling. *Mater. Res. Bull.* **2013,** *48*, 3351-3356.

32. Horikawa, T.; Do, D. D.; Nicholson, D., Capillary Condensation of Adsorbates in Porous Materials. *Adv. Colloid Interface Sci.* **2011,** *169*, 40-58.

33. Schwenzer, B.; Wang, L.; Swensen, J. S.; Padmaperuma, A. B.; Silverman, G.; Korotkov, R.; Gaspar, D. J., Tuning the Optical Properties of Mesoporous TiO_2 Films by Nanoscale Engineering. *Langmuir* **2012,** *28*, 10072-10081.

34. Lee, Y.-F.; Chang, K.-H.; Hu, C.-C.; Lin, K.-M., Synthesis of Activated Carbon-Surrounded and Carbon-doped Anatase TiO_2 Nanocomposites. *J. Mater. Chem.* **2010,** *20*, 5682-5688.

35. Lin, Y.-H.; Tseng, T.-K.; Chu, H., Photo-catalytic Degradation of Dimethyl Disulfide on S and Metal-ions Co-doped TiO_2 under Visible-light Irradiation. *Appl. Catal. A* **2014,** *469*, 221-228.

36. Liu, K.; Zhou, W.; Shi, K.; Li, L.; Zhang, L.; Zhang, M.; Fu, H., Influence of Calcination Temperatures on the Photocatalytic Activity and Photo-induced Hydrophilicity of Wormhole-like Mesoporous TiO_2. *Nanotechnol.* **2006,** *17*, 1363.

37. Fattakhova-Rohlfing, D.; Wark, M.; Brezesinski, T.; Smarsly, B. M.; Rathouský, J., Highly Organized Mesoporous TiO_2 Films with Controlled Crystallinity: A Li-insertion Study. *Adv. Funct. Mater.* **2007,** *17*, 123-132.

38. Dewalque, J.; Cloots, R.; Mathis, F.; Dubreuil, O.; Krins, N.; Henrist, C., TiO_2 Multilayer Thick Films (up to 4 μm) with Ordered Mesoporosity: Influence of Template on the Film Mesostructure and Use as High efficiency Photoelectrode in DSSCs. *J. Mater. Chem.* **2011,** *21*, 7356-7363.

39. Ohno, T.; Akiyoshi, M.; Umebayashi, T.; Asai, K.; Mitsui, T.; Matsumura, M., Preparation of S-doped TiO_2 Photocatalysts and Their Photocatalytic Activities under Visible Light. *Appl. Catal. A* **2004,** *265*, 115-121.

40. Shi, Z.; Liu, G.; Sun, N.; Yao, S.; Wang, S., Preparation and Characterization of Sulfur-Modified Mesoporous Titania Photocatalyst. *Russian J. Phys. Chem. A* **2013,** *87*, 1300-1305.

41. Guan, K., Relationship between Photocatalytic Activity, Hydrophilicity and Self-cleaning Effect of TiO_2/SiO_2 films. *Surf. Coatings Technol.* **2005,** *191*, 155-160.

42. Sakai, N.; Fujishima, A.; Watanabe, T.; Hashimoto, K., Enhancement of the Photoinduced Hydrophilic Conversion Rate of TiO_2 Film Electrode Surfaces by Anodic Polarization. *J. Phys. Chem. B* **2001,** *105*, 3023-3026.

43. Yu, J.; Zhao, X., Effect of Surface Treatment on the Photocatalytic Activity and Hydrophilic Property of the Sol-gel Derived TiO_2 Thin films. *Mater. Res. Bull.* **2001,** *36*, 97-107.

44. Tang, J.; Wu, Y.; McFarland, E. W.; Stucky, G. D., Synthesis and Photocatalytic Properties of Highly Crystalline and Ordered Mesoporous TiO_2 Thin Films. *Chem. Commun.* **2004,** 1670-1671.

45. Bian, Z.; Zhu, J.; Wang, S.; Cao, Y.; Qian, X.; Li, H., Self-assembly of Active Bi_2O_3/TiO_2 Visible Photocatalyst with Ordered Mesoporous Structure and Highly Crystallized Anatase. *J. Phys. Chem. C* **2008,** *112*, 6258-6262.

46. Li, G.; Zhang, D.; Yu, J. C., Thermally Stable Ordered Mesoporous CeO_2/TiO_2 Visible-Light Photocatalysts. *Phys. Chem. Chem. Phys.* **2009,** *11*, 3775-3782.

47. Min, X.; Li, H.; Jian-Qiang, W.; Ying, W.; Ling, G.; Jian-hua, Z.; Zhi-Gang, Z., The Direct Synthesis of Mesoporous Structured MnO_2/TiO_2 Nanocomposite: a Novel Visible-light Active Photocatalyst with Large Pore Size. *Nanotechnol.* **2008,** *19*, 185604.

48. Soler-Illia, G. J. de A. A.; Sanchez, C.; Lebeau, B.; Patarin, J., Chemical Strategies to Design Textured Materials: from Microporous and Mesoporous Oxides to Nanonetworks and Hierarchical Structures. *Chem. Rev.* **2002,** *102*, 4093-4138.

49. Farouk, H. U.; Raman, A. A. A.; Daud, W. M. A. W., TiO_2 Catalyst Deactivation in Textile Wastewater Treatment: Current Challenges and Future Advances. *J Ind. Eng. Chem.* **2016**, *33*, 11-21.

50. Tang, Y. C.; Hu, C.; Wang, Y. Z.; Zhang, H. P.; Huang, X. H., Progress in Deactivation of Titanium Oxide Photocatalyst. *Prog. Chem.* **2005**, *17*, 225-232.

TOC graphic

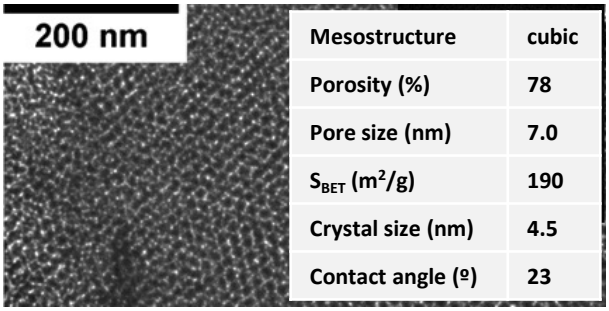

Mesostructure	cubic
Porosity (%)	78
Pore size (nm)	7.0
S_{BET} (m^2/g)	190
Crystal size (nm)	4.5
Contact angle (º)	23